Optimal Design and Integration of Decentralized Electrochemical Energy Storage with Renewables and Fossil Plants

Journal:	*Energy & Environmental Science*
Manuscript ID	EE-ART-03-2022-000771.R1
Article Type:	Paper
Date Submitted by the Author:	14-Jun-2022
Complete List of Authors:	Zantye, Manali S.; Texas A&M University Artie Mcferrin Department Of Chemical Engineering Gandhi, Akhilesh; Texas A&M University Artie Mcferrin Department Of Chemical Engineering Wang, Yifan; West Virginia University Vudata, Sai Pushpitha; West Virginia University Bhattacharyya, Debangsu; West Virginia University, Chemical Engineering Faruque Hasan, M.; Texas A&M University Artie Mcferrin Department Of Chemical Engineering,

SCHOLARONE™
Manuscripts

Optimal Design and Integration of Decentralized Electrochemical Energy Storage with Renewables and Fossil Plants

Manali S. Zantye[1], Akhilesh Gandhi[1], Yifan Wang[2], Sai Pushpitha Vudata[2], Debangsu Bhattacharyya[2], M. M. Faruque Hasan[1*]

[1]Artie McFerrin Department of Chemical Engineering, Texas A&M University
College Station, TX 77843-3122, USA.

[2]Department of Chemical and Biomedical Engineering, West Virginia University
Morgantown, WV 26506, USA.

Abstract

Increasing renewable energy requires improving the electricity grid flexibility. Existing measures include power plant cycling and grid-level energy storage, but they incur high operational and investment costs. Using a systems modeling and optimization framework, we study the integration of electrochemical energy storage with individual power plants at various renewable penetration levels. Our techno-economic analysis includes both Li-ion and NaS batteries to encompass different technology maturity levels. A California case-study indicates localized integration to be cost-effective for greater grid flexibility. Li-ion can mitigate the residual demand fluctuations of small to medium-sized plants, while NaS batteries would be best-suited for larger storage with higher renewable penetration. Overall, the battery-enabled renewable integration could reduce the the unmet grid demand by 75%, the renewable curtailment by 58%, and the CO_2 emission intensity by 16% while including the life cycle emissions of the battery and the renewable farm. Our scenario-based analysis also indicates that rather than replacing all fossil power plants, it is more economical to combine batteries and renewables with individual fossil plants to achieve a clean energy grid.

Keywords: Clean Energy, Simultaneous Design and Operation, Decentralized Integration, Optimization, Batteries.

*Correspondence should be addressed to M.M. Faruque Hasan at hasan@tamu.edu, Phone: (979) 862-1449.

1 Introduction

As the world's energy demand grows, there is a push to adopt carbon-neutral energy sources to counter the rising CO_2 emissions from the fossil fuel-dominant power sector. Renewable energy is inherently cleaner and more sustainable than fossil fuels. Owing to technological improvements and policy efforts, the contribution of renewable energy in the U.S. power generation mix has nearly doubled over the past decade. Nearly 90% of this growth can be attributed to the variable renewable energy (VRE) sources of wind and solar.[1] However, a major challenge towards widespread implementation of VRE sources is their spatio-temporal variability and non-dispatchability. During abundant solar energy production in the day, fossil-based electricity generators have to reduce their production to accommodate the excess solar energy. These generators are then required to rapidly increase their outputs to meet the peak evening demand when limited solar power is available. This leads to a 'duck' shape appearance of the residual energy demand curve, with the belly of the duck representing the low afternoon energy loads and the high evening loads depicted by the arch or the neck.[2] The rapid changes in the residual loads require electricity grid operators to carefully balance the energy supply and demand to avoid electricity undersupply as well as overproduction. Thus, maintaining electricity grid reliability under high renewable penetration scenarios requires additional measures to increase the flexibility of electricity grids.

Promising methods to achieve grid flexibility include the cycling of conventional generating units, curtailment of excess renewable energy, demand-side response, expanding transmission capabilities, and energy storage. Among these, power plant cycling and energy storage are the most effective measures to ensure grid flexibility.[3,4] The cycling of conventional natural gas-fired (NGCC) and coal-fired thermal power plants provides fast load-following capabilities to meet fluctuating demands. However, the rapid ramp-up/ramp-down of power output and the frequent startup/shutdown induce thermal and mechanical stresses to critical components such as the boilers and turbines.[5] The increased wear and tear increases the operating and maintenance costs by 2-5%, and reduces the plant lifetime.[6,7] Furthermore, the partial load operation of conventional units that are typically designed for base-load operation reduces the power generation efficiency and increases both the fuel consumption and CO_2 emissions.[8]

Energy storage ensures long-term grid reliability by decoupling the supply and the demand of energy. Integration of energy storage is typically considered at the grid-scale[9–11] or with a renewable generation facility[12–16]. However, this requires large storage capacities to effectively manage energy supply-demand fluctuations. For instance, to enable 20% renewable penetration in the grid, an estimated storage capacity of 200 GW/1000 GWh would be required to provide peak shaving capabilities.[17] The integration at grid-scale also requires capital-intensive modifications to the grid infrastructure. Furthermore, a limited number of storage technologies are currently suitable for large-scale energy storage considering the large power capacity and the long-duration discharge requirement. These primarily include pumped hydrostorage and compressed air energy

storage, which are often geographically limited.

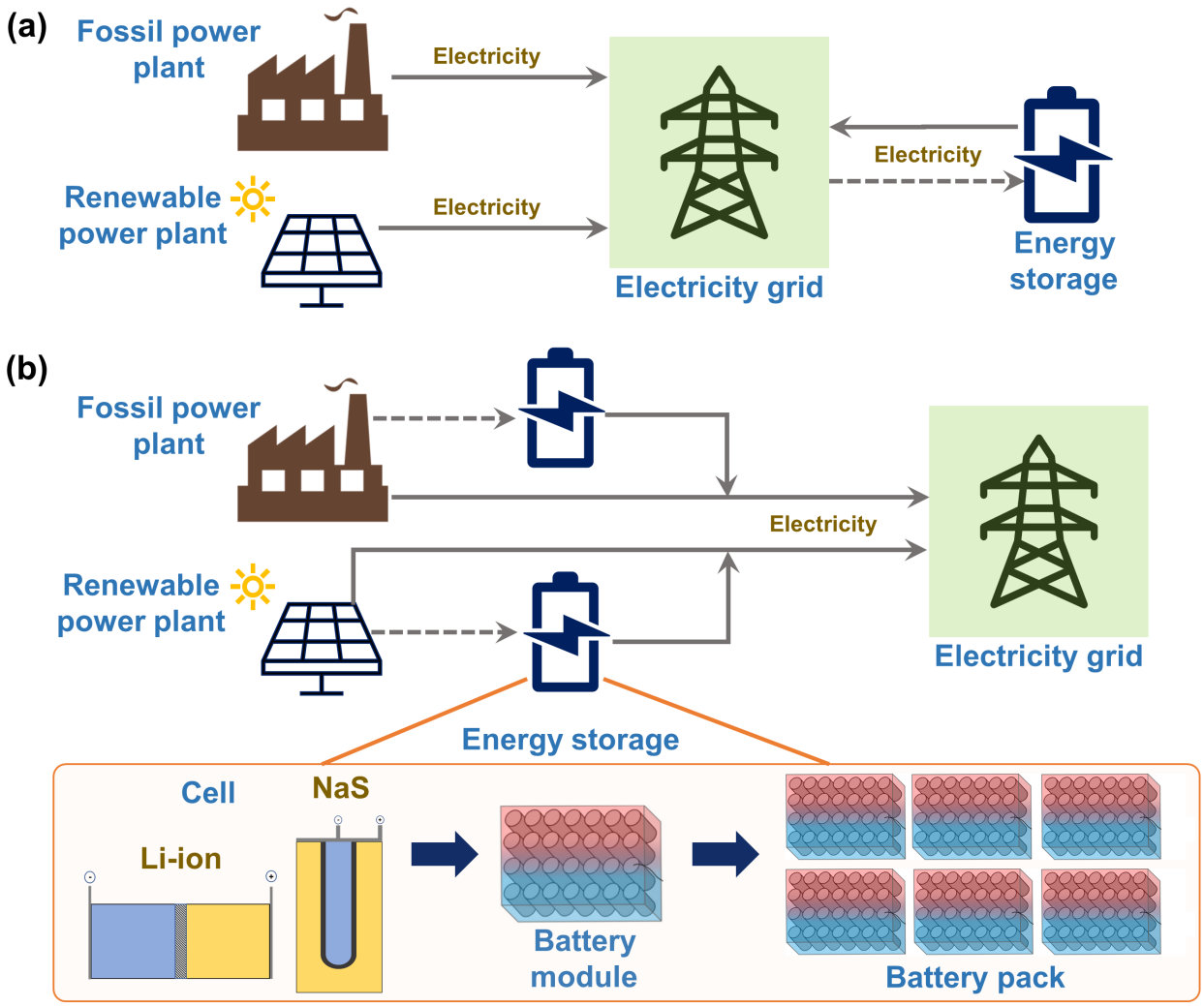

Figure 1: Two configurations of power generation systems and energy storage integrated with electricity grids. (a) Independent, grid-level integration of fossil power plants, renewable energy power plants and energy storage, and (b) Localized integration of energy storage with individual power plants. The electrochemical energy storage is comprised of several Li-ion/NaS cells, which form a battery module. A combination of several modules forms the entire battery pack.

Figure 1a depicts the conventional view of integrating energy storage at the grid-scale, which is independent of the power generation systems. This results in conservative costs and limited operational flexibility. The challenges associated with both the power generation and storage systems to mitigate renewable intermittency can potentially be addressed by the localized integration of energy storage with individual power plants as shown in Figure 1b. There are several benefits to considering the localized integration. Firstly, the operational synergies that exist between the energy storage system and the host power plant can be leveraged to attain increased flexibility of the conventional generating units for accommodating variable renewable energy. During periods

of significant renewable availability and resulting low net demand, some of the excess power plant output can be stored locally. On the other hand, for peak demand periods and low renewable availability, the stored power can be discharged to meet the net demand. This can reduce the cycling rates for fossil energy plants while at the same time ensuring power supply-demand balance in grids with high renewable penetration. Secondly, it broadens the scope of candidate storage technologies for the integration, which is otherwise limited by the required storage dynamics pertaining to grid-level integration. Thirdly, it allows faster response times to fluctuations in the grid electricity demand as compared to the conventional analysis. Since storage technologies such as batteries can respond within seconds as opposed to the minute-long response of even the fastest power plants such as NGCCs, the power plants can provide instantaneous response to demand fluctuations with a locally-integrated storage system. The localized integration also potentially requires lower storage capacities and can eliminate significant changes to grid infrastructure, thereby reducing the capital investment of storage integration.

Majority of the works focusing on the integration of energy storage with coal or natural gas-based thermal power plants consider storing the excess energy as steam.[18] Wojcik and Wang[19] considered thermal storage to improve the flexibility of a subcritical oil-fired conventional power plant while operating the plant close to design conditions. Mehrpooya et al.[20] performed an exergy analysis of a molten salt-based thermal storage system and a solar thermal field coupled with a conventional combined cycle power plant. Li and Wang[21] performed dynamic modeling and simulation of a supercritical pulverized coal-fired power plant integrated with high-temperature thermal storage (HTTS). They proposed three HTTS charging strategies and two HTTS discharging strategies to demonstrate increased load-following flexibility of the power plant. Richter et al.[22] showed benefits in using thermal energy storage for improving the operational flexibility of the plant while minimizing the cycling by maintaining a constant firing rate. Angerer et al.[23] considered the use of sensible heat storage to decouple the gas turbines and the heat recovery steam generators (HRSG) of an NGCC plant. Through transient simulation of the integrated process, they demonstrated that the thermal storage reduces the dynamic operation of the power plant and thereby reduces the fatigue-induced damage to critical plant components by 90%. Computational studies by Li et al.[24] and Rashid et al.[25] further reinforced the promise shown by decentralized thermal energy storage systems for the operation of natural gas power plants at rated load conditions in fluctuating electricity markets.

Electrochemical energy storage using batteries and chemical storage using hydrogen production has also been considered for the integration. Kim et al.[26] presented a dynamic optimization approach to determine the optimal dispatch of an integrated system comprised of a coal power plant, NGCC plant, NaS battery, and renewable energy. They considered minimizing the total cost of dispatch and included constraints for limiting the damage to the NGCC plant steam drum. Interestingly, their findings indicate that the flexibility of the system to meet changes in load demand is provided mostly by the NGCC plant, whereas NaS batteries are used sparingly and are

only deployed for scenarios with extreme ramp rates. The integration of Li-ion batteries with coal power plants can speed up the primary frequency control response as well as reduce the damage to power plant turbomachinery.[27] Zachar et al.[28] examined policy effects on the optimal design of an 'islanded' microgrid power system comprised of fossil fuel-based power production sources, lead-acid batteries and renewables. Allman and Daoutidis[29] explored the synergies between distributed renewable fuels and power systems through a framework for design optimization of a combined biorefinery and a microgrid with hydrogen energy storage. There has also been a growing emphasis on the localized integration of CO_2 capture systems with existing power plants to act as an 'indirect energy storage' mechanism for mitigating renewable intermittency.[30–33] This is achieved by flexible scheduling of the energy-intensive solvent regeneration process synergistically with renewable availability.

The dynamics of the power plant and energy storage as well as the spatio-temporal variability exhibited by the electricity markets and the renewable energy availability impact the storage size and integration economics. This necessitates the formulation of an optimization-based approach to consider the trade-offs between the cost and flexibility introduced by energy storage, as well as determine the integrated system operation under electricity demand and renewable fluctuations. In this work, we study a decentralized system of a power plant integrated with electrochemical energy storage. We consider two different types of electrochemical storage technologies: the mature and widely-used technology of lithium-ion (Li-ion) batteries and a developing, albeit promising technology in the form of sodium sulfur (NaS) batteries. Specifically, we investigate the optimal storage size for an existing NGCC power plant such that the benefits from the integration outweigh the upfront investment cost of the battery. We develop an optimization-based framework to evaluate the optimal integration decisions. To ensure that the system meets a time-varying grid demand, we model the time-varying operations of the power plant and energy storage. The presence of discrete and time-varying continuous decisions and the interactions between the system components result in a highly complex and large-scale model. To that end, we develop surrogate models for energy storage based on high-fidelity models. We apply the optimization-based framework for single power plants considering various demand profiles, as well as for power plants at a statewide scale with varying nominal capacities across California, U.S. The framework is then extended to the decentralized integration with renewable energy power plants and the battery integration results are compared. We address the following questions through our overall analysis:

1. For given NGCC power plants, what are the optimal integration decisions under the spatio-temporal variability of grid electricity demand and renewable availability? How are these transferable for renewable power plants?

2. How does the variability in the grid demand resulting from different penetration levels of renewables affect the selection of electrochemical energy storage?

3. What are the economic/operational benefits obtained from the battery integration?

4. What is the added cost of going 100% renewable coupled with battery-based energy storage?
5. Which electrochemical energy storage technology is more economical and beneficial for decentralized integration?
6. How do the battery size and economics change as we move from a single power plant analysis to a statewide study for different power plants?
7. Which decentralized configuration is the most economical and sustainable to ensure that the grid electricity demand is met while incorporating variable renewable energy: (i) integration of battery with existing NGCC plants, (ii) integration of renewable energy and battery with existing NGCC plants, or (iii) replacement of existing NGCC plants with renewable energy and battery systems?

Our mathematical programming-based optimization framework incorporating the battery and power plant models accounts for the trade-offs between the storage system cost and flexibility in decision-making. It also enables us to systematically evaluate the various differences between the technologically mature Li-ion technology and the promising NaS technology for the decentralized storage application. Specifically, we compare the two battery technologies in terms of different factors such as the high maturity of the Li-ion battery technology, and the long storage duration and lifetime offered by NaS batteries. This facilitates the assessment of the most-suitable electrochemical technology for the decentralized integration with power plants under varying demand and cost scenarios.

This article is structured as follows: Section 2 describes the overall methodology and the mathematical modeling-based framework for the decentralized integration of batteries with individual power plants. This is also used to study the optimal energy storage investment decisions as well as the dynamic system operation. Section 3 discusses the results from the application of the optimization framework for various case studies. Finally, Section 4 summarizes the key findings of the work.

2 Methodology

As depicted by Figure 1b, the integrated system is connected to the electricity grid such that it is required to satisfy the time-varying power demand of the grid. We define the problem statement for optimization as follows: subject to a time-varying profile of net electricity demand of the grid, determine the optimal system design and dynamic operation for the integration of NaS/Li-ion batteries with existing power plants which minimizes the total integrated system cost of meeting the net demand over a specified time horizon. The net demand for power plants is considered to incorporate the variability of renewable energy, and is given by the total electricity demand of the grid less the renewable generation. The design decision of the optimization framework comprises

of the battery size. The dynamic operating decisions include (i) the battery operating state i.e., charging, discharging or idle, (ii) the power output of the battery, and (iii) the power output of the power plant.

The optimization objective is to simultaneously determine the long-term investment decision of the battery integration capacity as well as the short-term operational decisions of the integrated system dynamic operation which minimize the overall system cost to meet the time-varying grid demand. To model and simulate the dynamic operation of batteries, there exist several classes of models including electrochemical models, equivalent circuit models and data-driven models. Electrochemical models are high-fidelity first principles-based models which incorporate the complex thermo-electrochemical and physical battery phenomena.[34,35] Although high-fidelity models accurately represent the dynamic battery operation, they introduce additional complexity when analyzing the integration with complex energy systems due to the highly non-linear representation of the underlying battery dynamics. To address this, simpler mathematical models known as equivalent circuit models are often employed for grid-level battery integration and analysis.[36–39] These models use common electrical circuit elements such as resistance, capacitance and voltage source to represent the battery electrochemical phenomena. The third category uses electrochemical simulation or experimental data to formulate 'black-box' battery models using data-driven techniques such as artificial neural networks (ANNs), recurrent neural networks (RNNs) and support vector machines (SVMs). Although these models show promise in accurately predicting the battery operation with low computational expense, they are mostly encountered in literature for Li-ion batteries, with few works focusing on the NaS battery application.[40–42]

In this work, we consider an equivalent circuit model to simulate the Li-ion battery behavior while lending computational tractability for the optimization. Furthermore, we develop a data-driven reduced-order model of the NaS battery derived from complex electrochemical models. This model incorporates the thermal management strategies required to make the NaS technology suitable for large-scale energy storage applications. Sections 2.1 and 2.2 elaborate on the working mechanism of the Li-ion and NaS battery technologies along with an overview of the reduced-order model development. The reduced-order models are then included in the overall optimization problem, which is given in Section 2.3 along with the key assumptions.

2.1 Li-ion Battery Model

The current market of energy storage and secondary batteries, in particular, is dominated by Li-ion battery storage. Li-ion batteries, which were first commercially developed for portable electronics, are now being increasingly used for diverse applications such as electric vehicles, military applications, medical devices and power tools. This massive growth can be attributed to their high energy density (300 Wh/kg) and high cell voltage (∼3.7 V) compared to most secondary batteries, along with their low self-discharge rates (0.1 - 0.3 %/day), fast response times (milliseconds) and high round-trip efficiency (95%).[43–45] However, despite the technological maturity and the promise

shown by Li-ion batteries, there still remains a gap in the use of this battery technology for utility-scale energy storage due to its limitation in providing long-duration energy storage, safety concerns associated with the tendency to overheat at high voltages, battery degradation which reduces the lifetime, and environmental issues linked to its production and recycling.[46–49]

The schematic of a Li-ion cell is depicted in Figure 2a. The typical Li-ion cell comprises of a graphite-based negative electrode or anode, and a lithium cobalt oxide ($LiCoO_2$)-based positive electrode or cathode. The half-cell reactions which take place in the anode (Eq. 1a) and cathode (Eq. 1b) during discharging, along with the overall cell reaction (Eq. 1c) are given by:

$$\mathrm{LiC_6} \leftrightarrow \mathrm{Li^+} + \mathrm{C_6} + \mathrm{e^-}, \tag{1a}$$

$$\mathrm{Li^+} + \mathrm{CoO_2} + \mathrm{e^-} \leftrightarrow \mathrm{LiCoO_2}, \tag{1b}$$

$$\mathrm{LiC_6} + \mathrm{CoO_2} \leftrightarrow \mathrm{C_6} + \mathrm{LiCoO_2}. \tag{1c}$$

The working mechanism of a Li-ion cell is different as compared to a conventional electrochemical process. The charge-discharge process is governed by an intercalation mechanism of the Li-ion in the crystalline lattice of the electrodes, as opposed to a traditional redox mechanism. When the cell is discharging, Li exits the surface of the graphite electrode layers, gives up an electron to the external circuit and enters the electrolyte in the form of Li^+. Li^+ travels to the positive electrode, where it accepts the electron from the external circuit to form Li, which enters the positive electrode particles at their surface. The opposite reaction occurs during charging. Along with the electrolyte which acts as a medium for Li^+ transport between electrodes, the Li-ion cell comprises of a separator. The separator acts as an electrical insulator to avoid charge transfer between the electrodes, and prevents the cell's self-discharge and internal short-circuit. The cell also includes current collectors which adhere to the electrodes and connect the battery to the external circuit.

A representative profile of the cell open-circuit voltage (OCV), which is defined as the terminal voltage when there is no flow of current, is depicted in Figure 2a.[50] The open-circuit voltage depends on the cell state of discharge (SOD). The cell SOD indicates the percentage of the overall capacity that has been discharged, with SOD value of 0 indicating that the cell is fully charged and SOD value of 100% indicating complete discharge. Conversely, the cell state of charge (SOC) is an indicator of the available cell capacity. As the cell is progressively discharged from the full-charge state, the OCV decreases steadily with an increase in the SOD. For high SOD levels, the OCV drops with only a small change in the SOD, requiring a careful discharge mechanism to avoid violation of the voltage limits.

We consider an equivalent circuit model (ECM) for the Li-ion battery technology where the battery dynamics are modeled using common electrical circuit elements. The specific ECM we consider is the Rint model, where an ideal voltage source represents the open-circuit voltage along with a series resistance to account for polarization, i.e. the departure of the cell terminal voltage from the open-circuit voltage under load.[51,52] The Rint model is a suitable model to capture

the nonlinear dynamics of Li-ion batteries while incorporating the OCV-SOC relationship and instantaneous voltage drop characteristics. It is proven to sufficiently capture the key phenomena in Li-ion batteries, accurately estimate the cell terminal voltage, while maintaining computational tractability[53] for the optimization problem. The detailed mathematical representation of the Rint model is presented in Section S2.1 of the Supplementary Information. The model is valid under the assumption that external thermal management strategies such as air cooling are employed to maintain the battery temperature at a constant ambient temperature of 25 °C.

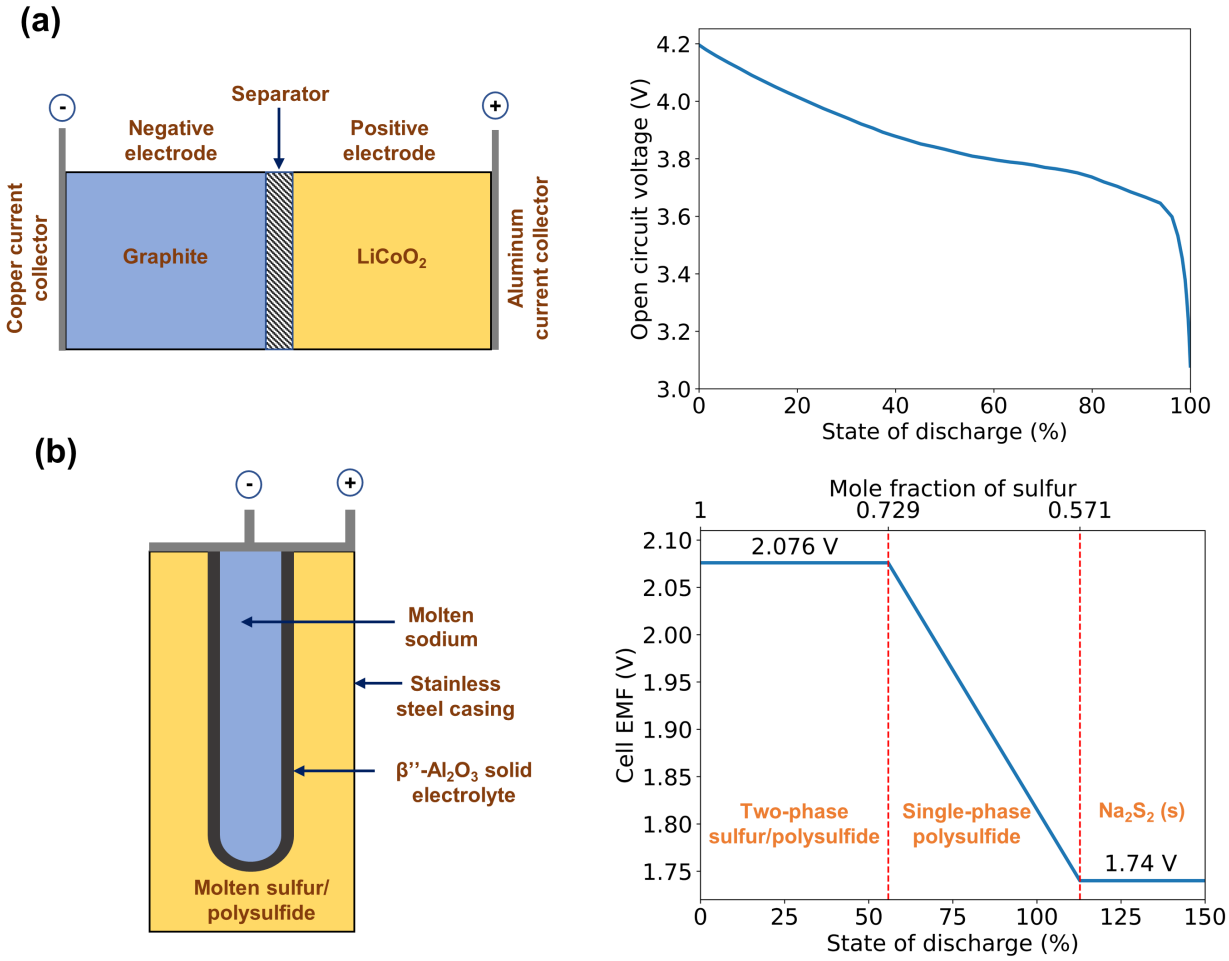

Figure 2: Schematic and voltage profiles of the Li-ion and NaS cells.[50,54–56] (a) The Li-ion cell open-circuit voltage (OCV) decreases as the cell is progressively discharged. (b) When the NaS cell is fully charged, the OCV is equal to the nominal voltage. As the cell discharges, a two-phase region starts forming in the cathode, which results in a voltage drop.

2.2 NaS Battery Model

NaS batteries, first commercially developed by the Tokyo Electric Power Co. (TEPCO) in collaboration with NGK insulators[57], are excellent candidates for cost-effective, large-scale stationary energy

storage due to their low cost of electrode materials, high open-circuit voltage (∼2 V), high theoretical energy density (150-240 Wh/kg), long cycling lifetime (over 10 years) and high round-trip efficiency (90%).[58–60] However, the conventional room-temperature operation of the NaS batteries shows poor capacity retention and cycling properties. To enable the use of this battery technology for large-scale storage applications, high-temperature NaS batteries with operating temperatures of 300 - 400 °C are typically considered.[61,62] Under these operating conditions, there is a risk of thermal runaway during high energy density operation. To address the thermal management issue of NaS batteries and make the technology suitable for large-scale storage applications, this work considers an active cooling strategy of the battery by the use of air as a cooling medium. Furthermore, the thermal management also has a strong influence on the internal cell resistance and voltage. To monitor this, the dynamic models of the NaS cell developed in this work consider the effect of temperature on the cell's physical properties.[63]

The typical configuration of a NaS cell is depicted in Figure 2b. Each NaS cell consists of molten sodium at the core which serves as the anode. This is separated from a molten sulfur cathode by a beta"-alumina solid ceramic electrolyte. The half-cell reactions in the cathode and anode, and the overall cell reaction are given by:[55,56]

$$2\,\mathrm{Na} \leftrightarrow 2\,\mathrm{Na}^{+} + 2\,\mathrm{e}^{-}, \tag{2a}$$

$$2\,\mathrm{Na}^{+} + \mathrm{x\,S} + 2\,\mathrm{e}^{-} \leftrightarrow \mathrm{Na_2S_x}, \tag{2b}$$

$$2\,\mathrm{Na} + \mathrm{x\,S} \leftrightarrow \mathrm{Na_2S_x}. \tag{2c}$$

The forward reactions take place during the discharge operation. As the cell discharges, the sodium donates an electron to the external circuit and migrates to the sulfur container where it reacts with sulfur to form sodium polysulfide. In the fully charged state, the cathode is entirely molten sulfur. As the extent of discharge increases, the composition of the sulfur electrode changes to two-phase comprising of molten sulfur and sodium polysulfide. For further cell discharge, a single-phase polysulfide region is formed in the cathode. This change in the composition of the sulfur electrode as the reactions proceed also affects the cell electromotive force (EMF). Figure 2b shows the cell EMF profile with increasing level of discharge and mole fraction of sulfur in the cathode. The cell EMF is relatively constant for two-phase region, but the formation of the single-phase region results in a drop in the cell EMF. As the cathode composition is a result of the extent of cell discharge, the cell SOD is an important cell state which determines its voltage and internal cell resistance.

Based on this working mechanism, reduced-order models for the NaS cell are developed based on the first principles models of Schaefer et al.[64] using a nonlinear time-series analysis method known as NAARX (nonlinear additive autoregressive with exogenous input).[65] The general form and description of the NAARX category of time-series models, along with a detailed overview of the model development process is given in Section S1 of the Supplementary Information. Due to

the different voltage profiles in the single-phase and two-phase regions of the sulfur electrode in the NaS cell, four different models are generated depending on the state of the sulfur electrode and the direction of power flow through the cell. Specifically, these models correspond to the following four states of the cell: single-phase charging, two-phase charging, single-phase discharging and two-phase discharging. The detailed mathematical representation of the NaS models is presented in Section S2.2 of the Supplementary Information.

On comparison of the parameters of the Li-ion and NaS battery technologies from Table S2, we find that the specific investment and fixed operating and maintenance (O&M) cost of Li-ion batteries is lower than NaS batteries. However, Li-ion also has lower lifetime and lower maximum storage duration compared to NaS batteries. Thus, through the inclusion of these models in the optimization framework, we aim to systematically decide the optimal integration decisions for a given power plant which account for the trade-off between the higher efficiency and the lower cost of Li-ion batteries, and the lower lifetime and less storage duration compared to the NaS technology. Note that each technology is evaluated in the optimization individually, and the optimization framework does not simultaneously include the models of both technologies. The overall optimization model formulation is given in the following section.

2.3 Simultaneous Design and Integration Model

The following assumptions preface the optimization model development:

- Startup and shutdown operation of the NGCC power plant is not considered. At any given time, the power plant operates between its minimum non-zero load and nominal capacity.
- All cells in the battery system have identical current, voltage and power output at any given time. Furthermore, the state of charge/discharge for all the cells is equal at any time.
- The integrated system is not required to exactly meet the grid demand. Any excess or deficit of electricity supply to the grid is then penalized and added to the cost.
- Degradation of the battery and the subsequent battery replacement is not modeled. To justify this assumption, we incorporate a low-end value of the battery lifetime along with conservative bounds on the battery operation. Similar assumptions have also been incorporated in previous systems-level studies which include batteries.[28,66]

The optimization formulation minimizes the total system cost of meeting the grid demand. The decision variables in the framework include the design of the battery and the time-varying operation of the battery and the power plant. The optimization model along with the mathematical representation of the decision variables, the dependent variables and the model parameters is presented in Section S3 of the Supplementary Information. The overall framework including the optimization model and the single cell models for the Li-ion and NaS technologies given in Sections 2.1 and 2.2 forms a mixed-integer nonlinear programming (MINLP) problem.

3 Results and Discussion

The optimization-based simultaneous design and operational scheduling framework is implemented for a time discretization of 10 minutes over a time horizon of one day to study the integration of energy storage with power plants. We consider case studies based on the state of California in the U.S. for the electricity market and renewable availability profiles. California is an important state to examine the effect of high renewable penetration on power systems, being the leading producer of renewable-generated electricity in the U.S. with more than half of the in-state electricity generation coming from renewable sources in 2019.[67] The net electricity demand profile is obtained for representative days from the California Independent System Operator's (CAISO) actual load data reports.[68] The net demand is reported for 5 minute time increments and represents the total system demand minus the wind and solar energy generation. This is converted to a 10 minute increment profile by averaging the data of adjacent time periods and scaling the profile using the NGCC plant's nominal capacity.

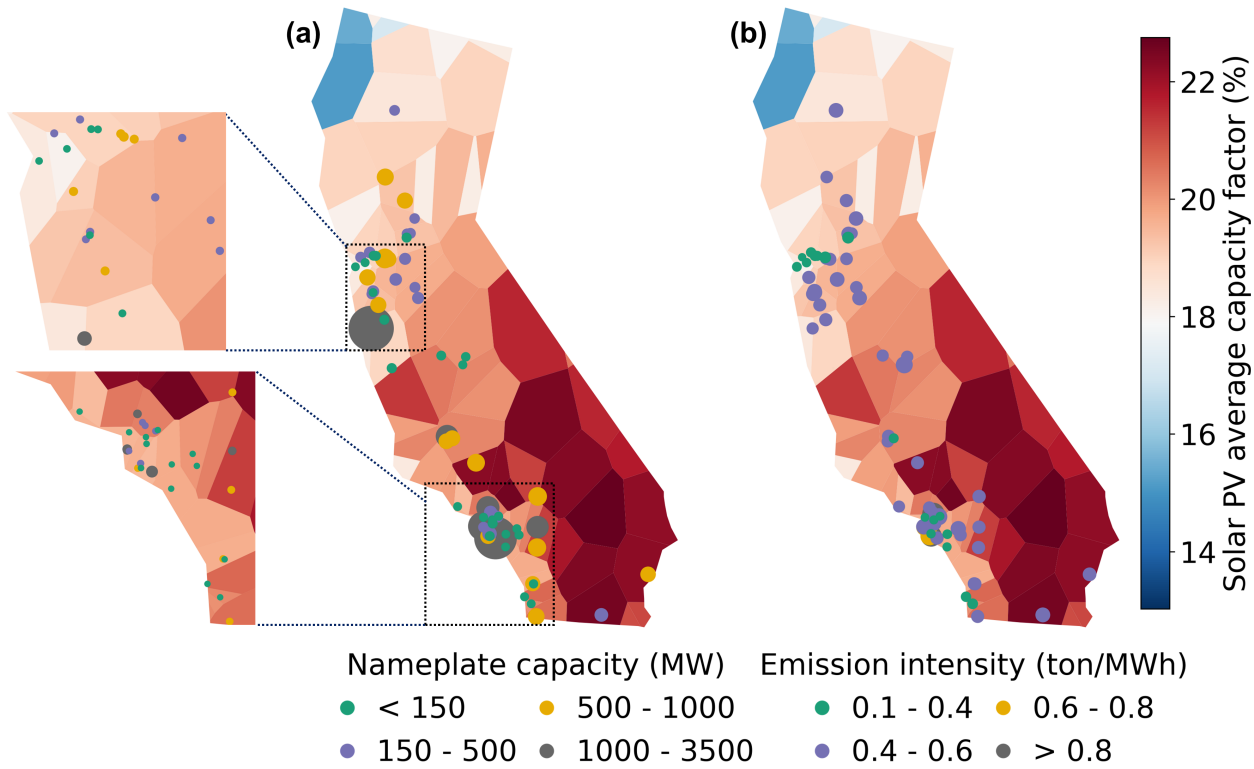

Figure 3: Variation of NGCC power plant data and solar availability across the state of California. The points on (a) represent the locations of the existing NGCC plants with the point size proportional to the plant nameplate capacity. The points on (b) represent the corresponding CO_2 emission intensities of the existing power plants. Solar PV capacity factors for the weather stations across the state are depicted using Voronoi polygons. We see that the state has high amounts of solar energy availability, making it important to address the integration issues arising from its spatio-temporal nature.

Data for the power plants' nameplate capacities and CO_2 emissions is obtained from the United States Environmental Protection Agency (U.S. EPA)'s latest Emissions & Generation Resource Integrated Database, eGRID2019, which was released in February 2021 demonstrating 2019 data.[69] According to the database, there are about 65 power plants in the state with operational NGCC units in 2019. For a power plant with NGCC listed as its primary generating unit in eGRID2019, we assume the NGCC nameplate capacity to be the same as that of the entire plant. This is because although the plant's generation mix may also include other fuel sources, its power production can be attributed majorly to its NGCC units. Figure 3a depicts the location of the power plants along with their nameplate capacities. Nearly 90% of the power plants have nameplate capacities below 1000 MW. The plant nameplate capacity serves as an input parameter $P^{nom,ng}$ in the optimization model of Section 2.3. Figure 3b represents the CO_2 emission intensity of the 65 power plants. 43 out of the 65 power plants have emission intensity in the range of 0.4 - 0.6 ton/MWh, which is the typical emission intensity for NGCC power plants.[70]

In addition to the power plant data, weather data for the solar irradiation is obtained for Typical Meteorological Year (TMY3) sites across California from the National Renewable Energy Lab (NREL)'s National Solar Radiation Database (NSRDB).[71] This dataset provides weather conditions for a typical, representative year based on historically observed conditions for different sites across the U.S. The solar irradiation data is converted to the corresponding solar PV capacity factor using the reference irradiation.[72] Specifically, the solar PV capacity factor is defined by the following equation:[30]

$$cf_t^{sp} = \frac{H_t}{H^{ref}} \eta^{arr} \eta^{ac/dc} \eta^{wir}, \ \forall t \in \mathcal{T}, \tag{3}$$

where, H_t denotes the actual solar irradiation at a given location at time t (in W/m^2), H^{ref} denotes the reference irradiation of the solar panel, and the parameters $\eta^{arr}\eta^{ac/dc}\eta^{wir}$ denote the efficiencies of the PV array, DC-to-AC conversion and wiring, respectively. For a reference irradiation of 1000 W/m^2 and a combined efficiency factor of 93.75%, the capacity factor is completely determined by the actual solar irradiation at a given time. The capacity factor of the solar panel is thereby pre-determined based on the solar availability for a given PV system configuration and is not a scheduling decision. The sole degree of freedom to regulate the amount of solar power output delivered is then the size of the solar farm. This is given by the following equation:

$$P_t^{sp} = cf_t^{sp} sz^{sp}, \ \forall t \in \mathcal{T}, \tag{4}$$

where, P_t^{sp} denotes the power output of the solar panel at time t (in MW), cf_t^{sp} is the capacity factor at time t and sz^{sp} is the size of the solar farm (in MW). Figure 3 also shows the statewide variation of the solar capacity factor representing the solar energy availability. We observe that the solar availability across the state is the highest in the nation, with regions in Southern California showing an annual average capacity factor of nearly 23%.

The framework is first demonstrated for the integration of batteries with NGCC power plants and then extended to consider the integration with renewable energy plants. We consider the following two cases for the integration with renewable plants: (i) existing NGCC power plants integrated with battery-enabled renewable energy farms, and (ii) replacement of the existing NGCC power plants with battery-integrated renewable energy farms. If the integration of renewable energy and/or battery systems is optimal, we consider that these systems are co-located with the NGCC plants. In all these cases, the location of the integrated renewable energy/battery facilities for each of the existing NGCC plants is the same as the location of the NGCC plant.

3.1 Integration with Fossil Power Plants

At the grid-level, increasing penetration of renewables increases the demand variability for fossil power plants. In other words, to mitigate the variability in renewable energy, fossil power plants need to vary/cycle their loads more frequently and more sharply. For a single NGCC power plant of 641 MW nominal capacity, we investigate how such increase in demand variability representing different levels of renewable penetration and steeper ramping requirements plays a role in the selection of battery storage technologies. The net demand profiles incorporating different degrees of variability are depicted in Figure 4a. The 'base-case' scenario refers to the nominal net load profile without any extreme ramp rates and demand fluctuations. As the amount of renewable shares increase, the net load during the day progressively decreases, with increasing demand during the peak evening hours.

The cost minimization objective minimizes the sum of the battery investment and the operating cost incurred if the battery integration is selected, the power plant variable operating cost, the plant cycling cost, and penalty on any imbalance between the integrated system power supply and grid demand. Considering the nominal values of the cost parameters, we find that it is optimal to not integrate a Li-ion or a NaS battery with the power plant for the base-case profile. In the absence of storage integration, the net demand is met by the power plant through ramping its output as well as operation at partial load conditions. Although there is a large amount of cycling, the resulting cycling cost is insignificant (0.2% of the total cost). This indicates that at the nominal cost parameters, the NGCC cycling cost is insufficient to compensate for the large battery investment to reduce the power plant cycling. Through a cost sensitivity study (Supplementary Information, Section S5.1), we find that the NGCC specific cycling cost should be significantly greater than the unit battery investment cost to achieve favorable economics of integration.

As the extent of renewable penetration is increased, we find that it is increasingly beneficial for the power plant to invest in a battery to meet the grid demand. Figure 4b shows the optimal battery integration sizes of the Li-ion and NaS technologies for the different levels of increase in renewable shares. Overall, the battery size increases with the renewable penetration. For Li-ion batteries, the size hits the upper bound of 400 MWh for a renewable penetration increase of 60% and beyond.

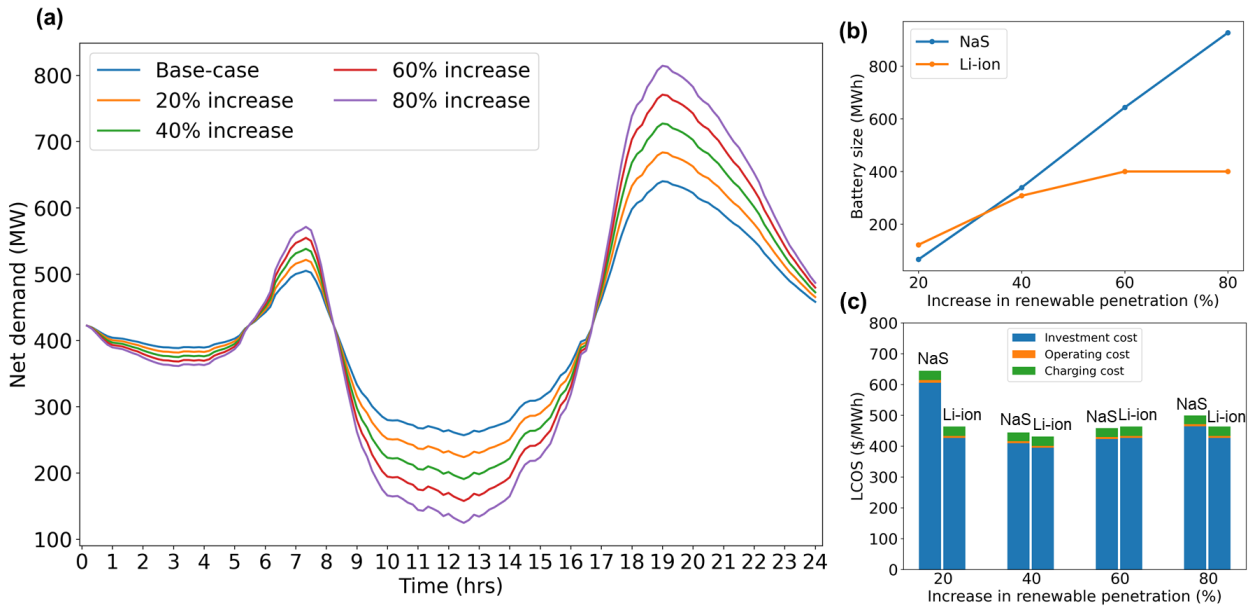

Figure 4: (a) Net demand profiles, (b) optimal battery size, and (c) battery cost at different renewable penetration levels. The investment cost forms a major portion of the total cost, followed by the charging cost and the cost of operating the battery. With an increase in the renewable penetration levels, the battery size increases for both technologies. This results in a decreasing trend in the LCOS up to a renewable penetration increase of 40%. Beyond a 40% increase in demand variability, the extent of battery overdesign increases, thereby resulting in an increase in the LCOS.

The corresponding operational profiles of the integrated system for the 80% change in the demand profile are depicted in Figure S4 of the Supplementary Information. The storage system is charged using the excess energy generated by the power plant during periods of low net demand in the middle of the day. The stored energy is then discharged to meet the demand peak during the evening hours. We also observe that the NaS battery exhibits a longer storage duration, which is 50% higher than the storage duration of the Li-ion battery. Although the batteries discharge in the evening hours to meet the demand peak, there is some fraction of the peak demand which is unmet. This is due to the operational limits imposed on the cell voltage and state which results in the underutilization of the storage capacity.

To analyze if the self-discharge mechanism of the battery affects these results, we extend the analysis to also include the self-discharge rate. A self-discharge rate of 0.2% per day is considered for Li-ion batteries.[73] The modified energy balance accounting for the self-discharge of the battery in the idle state is provided in Section S2.1 of the Supplementary Information. We find that the self-discharge has a negligible effect on the optimal solution. For instance, to compensate for the loss of energy due to self-discharge, the amount of energy charged to the battery increases by 0.0006%, while the amount of energy discharged by the battery during peak hours reduces by 0.006%. Overall, this results in a $10 per day increase in the total system cost. Thus, due to

the battery not being in the idle state for extended periods and the low self-discharge rate of the considered battery technologies, the effect of including the self-discharge mechanism on the overall results is negligible.

The economic benefits of the battery system are assessed by measuring the levelized cost of storage (LCOS). LCOS represents the discounted cost to discharge one unit of electrical energy from the battery system. The LCOS is calculated based on the optimization results with the detailed mathematical representation shown in Section S4 of the Supplementary Information. Figure 4c depicts the battery LCOS at the different renewable penetration levels. With the increase in renewable penetration levels, the LCOS for both the storage technologies decreases for up to 40% increase in renewable penetration, and then increases. This indicates that the battery is increasingly overdesigned beyond the 40% level. Overall, the average capacity utilization of NaS batteries is 38% higher than the capacity utilization of Li-ion batteries. On comparison of the cost of the two technologies from Figure 4c, we find that the LCOS of the NaS battery is higher than the LCOS of Li-ion for the demand variability increase levels of 20%, 40% and 80%. An interesting observation is for the 60% level, where the LCOS of NaS is lower than that of Li-ion. Thus, the lower lifetime and the lower storage duration coupled with the lower utilization of Li-ion technology compared to NaS batteries for these demand scenarios outweigh the cost benefits obtained from the lower investment cost of Li-ion batteries, contributing to an overall higher LCOS.

3.1.1 Statewide integration

The analysis for the single power plant case is expanded to a statewide study for NGCC power plants across California. We observe that for the nominal net demand profile, the battery integration is not optimal for any of the 65 power plants in the state. The net demand is met exactly by all the plants, thereby resulting in no electricity oversupply and undersupply costs. Next, we extend the analysis to consider demand scenarios with increasing variability from the nominal profile, i.e. 20%, 40%, 60% and 80% increase in renewable penetration. We observe that the battery selection is optimal at the higher demand variability, and the battery integration size increases with both the NGCC nominal capacity and the level of increase in demand variability (Supplementary Information, Figure S5).

The corresponding system cost in terms of the levelized cost of electricity (LCOE) for the integrated system and the LCOS for the different levels of increase in renewable penetration is given in Figure 5 for the representative case of NaS battery. The LCOE represents the net present costs incurred by the integrated system to generate one unit of electricity. The detailed mathematical representation of the LCOE is presented in Section S4 of the Supplementary Information. From Figure 5a, we can see that the LCOE with battery selection shows an increasing trend with the nameplate capacity of the power plant and the renewable penetration level. We also observe that the average LCOS shows a decreasing trend as we increase the extent of renewable integration, making the decentralized battery integration more economical at higher renewable penetration levels. In addition, the battery integration results in an average of 18% reduction in the NGCC

variable operating cost, and an average of 53% reduction in the unmet demand as compared to the stand-alone NGCC plant (Supplementary Information, Figure S6).

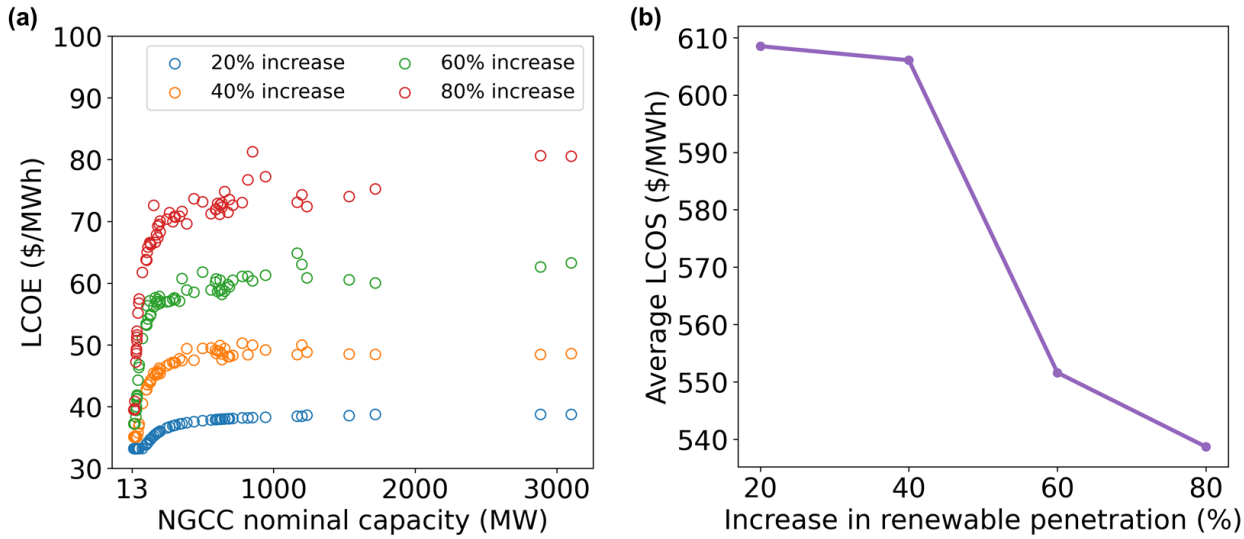

Figure 5: Integrated system cost represented by (a) LCOE and (b) average battery LCOS for 20%, 40%, 60% and 80% increase in renewable energy penetration considering NaS battery integration.

As the integration of the NaS and Li-ion storage technologies is considered independently of each other in the optimization, we perform a comparison of the technologies using the post-calculated LCOE metric. Figure 6a depicts the NGCC nominal capacities and demand scenarios for which the LCOE with Li-ion battery integration is less than that with NaS battery integration, i.e. the Li-ion battery integration is more beneficial compared to NaS. Conversely, Figure 6b represents the cases which facilitate more favorable economics of NaS battery integration compared to Li-ion. Overall, we observe that there is a higher number of data points that favor Li-ion integration. Furthermore, NaS battery integration is observed to be more beneficial at higher levels of renewable penetration and for larger-sized power plants. This is due to the high maximum storage capacity and storage duration required to meet the demand for these cases, which is provided by NaS batteries. On the other hand, Li-ion integration is observed to be more beneficial for medium-sized power plants. In addition, Figure 6c shows the cases where the integration of neither battery technology is optimal. There are a total of 16 power plants with capacities below 74 MW for which the battery selection is not optimal for varying levels of renewable penetration. For lower renewable penetration levels, a Li-ion/NaS battery is not selected for a larger range of NGCC nominal capacities.

The statewide average LCOE of the integrated system with Li-ion integration is shown in Figure 7 in comparison with the average LCOE with NaS battery integration. We find that the LCOE considering NaS battery integration is on an average a mere 5% higher than that considering Li-ion battery integration. Thus, although the specific investment cost of Li-ion battery is 65% less than the specific investment cost of NaS battery, the lower storage duration and lower lifetime of Li-ion technology result in marginal cost benefits obtained from the Li-ion battery integration

compared to the NaS battery integration. This suggests that further reduction in the investment cost of the NaS battery through technological improvements can potentially result in the integrated system LCOE with NaS battery integration being lower than that with Li-ion battery integration. Next, we extend this analysis to the integration of batteries with renewable energy power plants and compare the results.

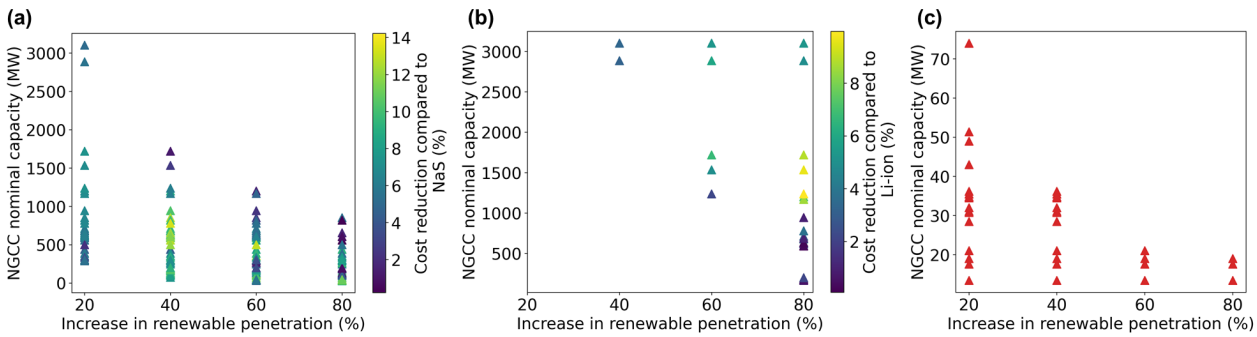

Figure 6: (a) Cases where Li-ion battery integration is more economical compared to NaS battery, (b) cases for which NaS battery integration is more economical compared to Li-ion, and (c) cases for which integration of neither battery technology is optimal. The percentage reduction in LCOE with respect to NaS for (a), and with respect to Li-ion for (b) is represented by the color of the data points.

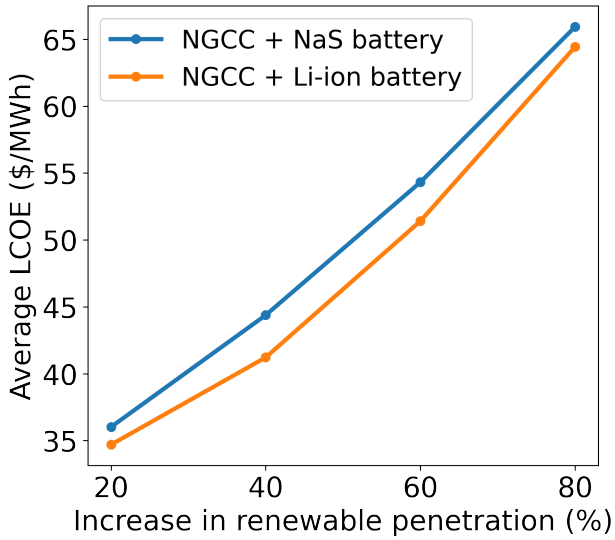

Figure 7: Average LCOE of the integrated system with NaS battery and Li-ion battery integration at different renewable penetration levels.

3.2 Integration with Renewable Power Plants

The system considered in our analysis so far is an NGCC power plant integrated with battery storage. The system is designed to be flexible enough such that it meets the time-varying net demand of the electricity grid under intermittent renewable integration. The variability of renewable

energy is incorporated implicitly in the framework through a scaled net demand profile of the electricity grid. In this section, we extend this analysis to also explicitly consider the renewable availability at each power plant location. We consider the following two cases for this study: (i) an existing NGCC power plant integrated with battery storage and a renewable energy farm, and (ii) replacement of an existing NGCC power plant with a renewable energy farm and battery storage. The specific renewable energy technology considered is solar PV, due to the promise shown by solar power in the state of California as well as the need to address the critical challenges arising from its overgeneration. From Figure 6, we see that there exist a higher number of power plants/demand scenarios where Li-ion battery integration is favorable over NaS. Based on this, we consider the battery type as Li-ion battery for the analysis.

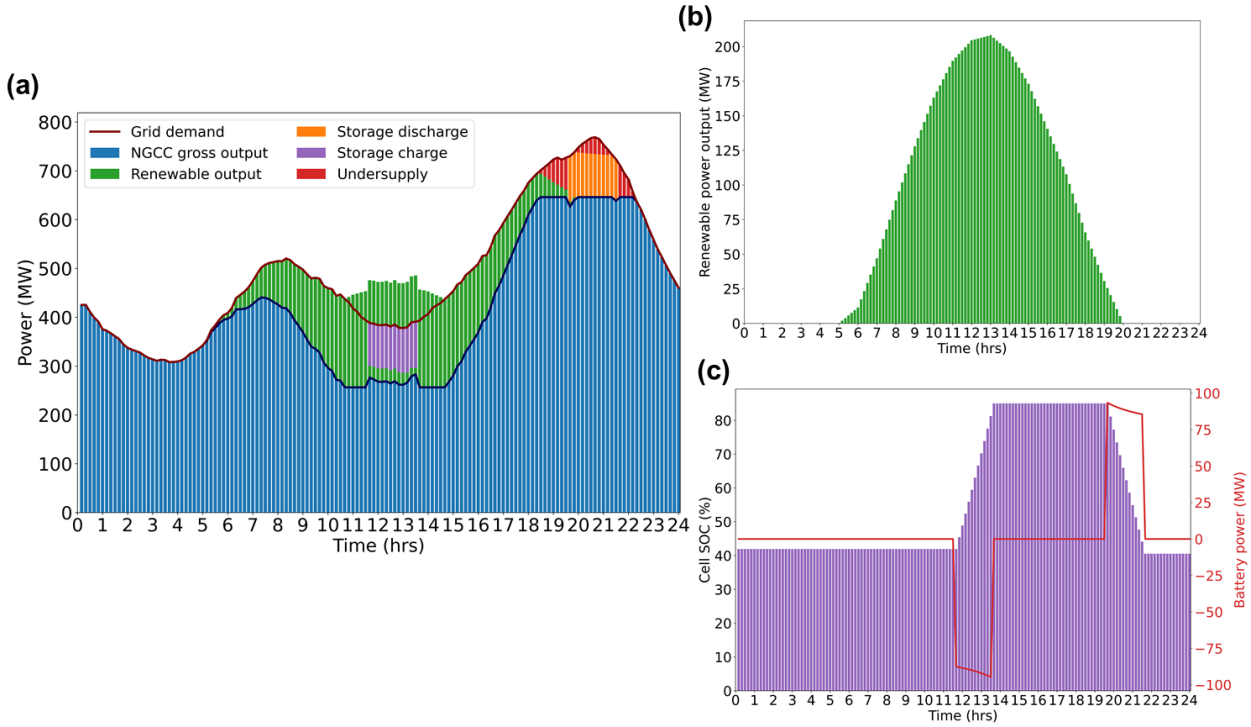

Figure 8: Optimal operational profiles for (a) integrated system comprising the power plant, renewable energy farm and Li-ion battery, (b) renewable energy farm, and (c) Li-ion battery system.

To begin with, the previously considered system configuration is extended to also consider a co-located renewable energy (solar PV) farm integrated with an existing NGCC power plant along with battery storage. In addition to the design decision of sizing the battery system, the sizing and operational decisions of the renewable energy farm are incorporated in the optimization framework. This enables us to study how the two power sources of fossil and renewable energy work in tandem to meet the electricity demand, while mitigating the intermittency of renewables using battery storage. We first consider the single NGCC power plant case with a nameplate capacity of 641 MW. In place of the net demand profile, here we consider the actual grid electricity demand profile with the renewable availability data considered for the city of Oakland in California. The demand

profile is scaled with respect to the plant nameplate capacity. Since renewable energy is included as an additional power source, the scaled demand profile is increased by 20%. The specific investment cost of solar PV is considered to be a futuristic value of $300 per kW.

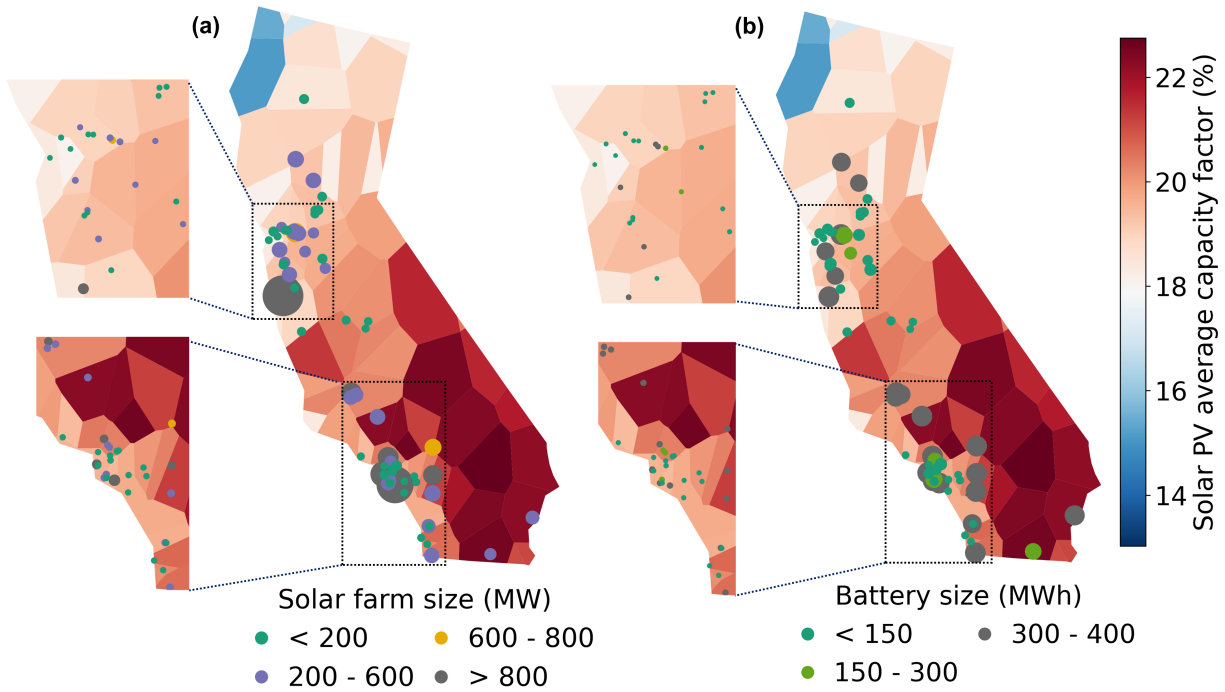

Figure 9: (a) Optimal renewable farm, and (b) optimal battery integration size with NGCC power plants across the state of California. Both the battery integration size and the renewable size increases with the NGCC nominal capacity. More than half of the power plants have a battery integration size less than 150 MWh and a co-located renewable farm size less than 200 MW.

Figure 8 shows the optimal system operation for a representative summer day. We find that it is optimal to integrate renewable energy with the 641 MW capacity NGCC power plant, with the co-located renewable energy farm sized at a capacity of 222 MW. It is also optimal to integrate a battery sized at its maximum capacity of 100 MW/400 MWh. On comparison with our previous analysis of Section 3.1, we find that the NGCC power plant operates at reduced capacity for a longer duration of time during the day, when renewable energy is readily available. During periods when there is a dip in the demand peak in the day, the excess renewable energy is stored by charging the battery. The stored energy is then discharged to meet the demand peak during evening hours, when the renewable output drops to zero.

We compare the cost obtained from this analysis with the 60% increase in net demand variability case of NGCC integration with battery alone. This scenario is considered as the peak net demand during periods of limited renewable availability is close to the peak demand values when the actual demand is increased by 20%. The optimal LCOS of the battery for the NGCC-renewables-battery system is $433 per MWh, which is 6.5% lower than the LCOS of the integration of battery with

the NGCC plant. The lower LCOS is due to the reduction in the charging cost of the battery. For the case of NGCC power plant integrated with battery alone, the power plant increases its power output to charge the battery system. Thus, there is a significant amount of charging cost due to the power generation cost of the plant. On the other hand, in the case of the NGCC plant integrated with a renewable energy farm and battery, the battery is charged using the excess renewable output, which has near-zero marginal production costs.

The analysis for the single power plant case is then extended to the different NGCC power plants across California. The data for solar energy at each power plant location is obtained from the weather station in its closest proximity, or the data for the corresponding Voronoi polygon it falls into (Figure 3). The optimal co-located renewable farm size and the battery integration size for the power plants across the state is given in Figure 9. We observe that both the renewable farm size and the battery integration size increases with the power plant nameplate capacity. In addition, the battery integration size shows a strong positive correlation to the renewable farm size (Pearson correlation coefficient of 0.78) and a moderate positive correlation to the average solar PV capacity factor (Pearson correlation coefficient of 0.34). This indicates that a bigger battery size is required to mitigate the intermittent power production of large renewable energy farms in regions with high amounts of renewable availability.

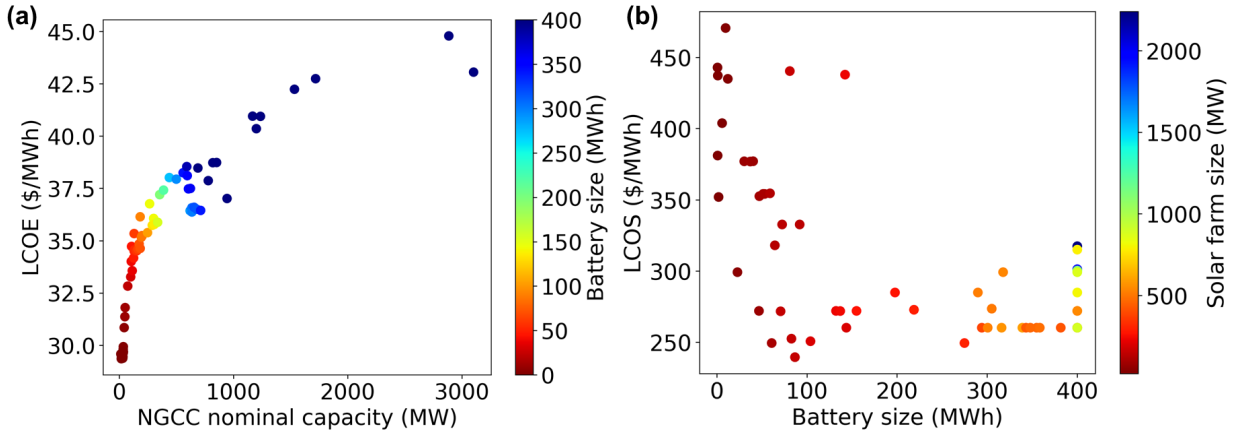

Figure 10: System cost represented by (a) LCOE and (b) battery LCOS for NGCC power plants across California integrated with renewables and battery.

Figure 10 shows the system costs in the form of the LCOE of the overall system and the LCOS of the battery. We find that the overall system LCOE increases with the NGCC nominal capacity and the battery integration size. On the other hand, the battery LCOS shows a roughly decreasing trend with the battery size. The average LCOE of the integrated system is $35 per MWh, while the average LCOS is $272 per MWh. The average LCOE for our previous study of NGCC plants integrated with battery alone was $51 per MWh for the 60% renewable penetration case (Figure 7), and the average LCOS was $444 per MWh. Although there is now an additional investment in the renewable energy farm, the total system cost is reduced by 18%, and the overall system LCOE is

reduced by 31% compared to the previous case. The reduction in the LCOE and total cost can be attributed to the additional power output of the renewable energy farm and the reduction in the electricity undersupply costs.

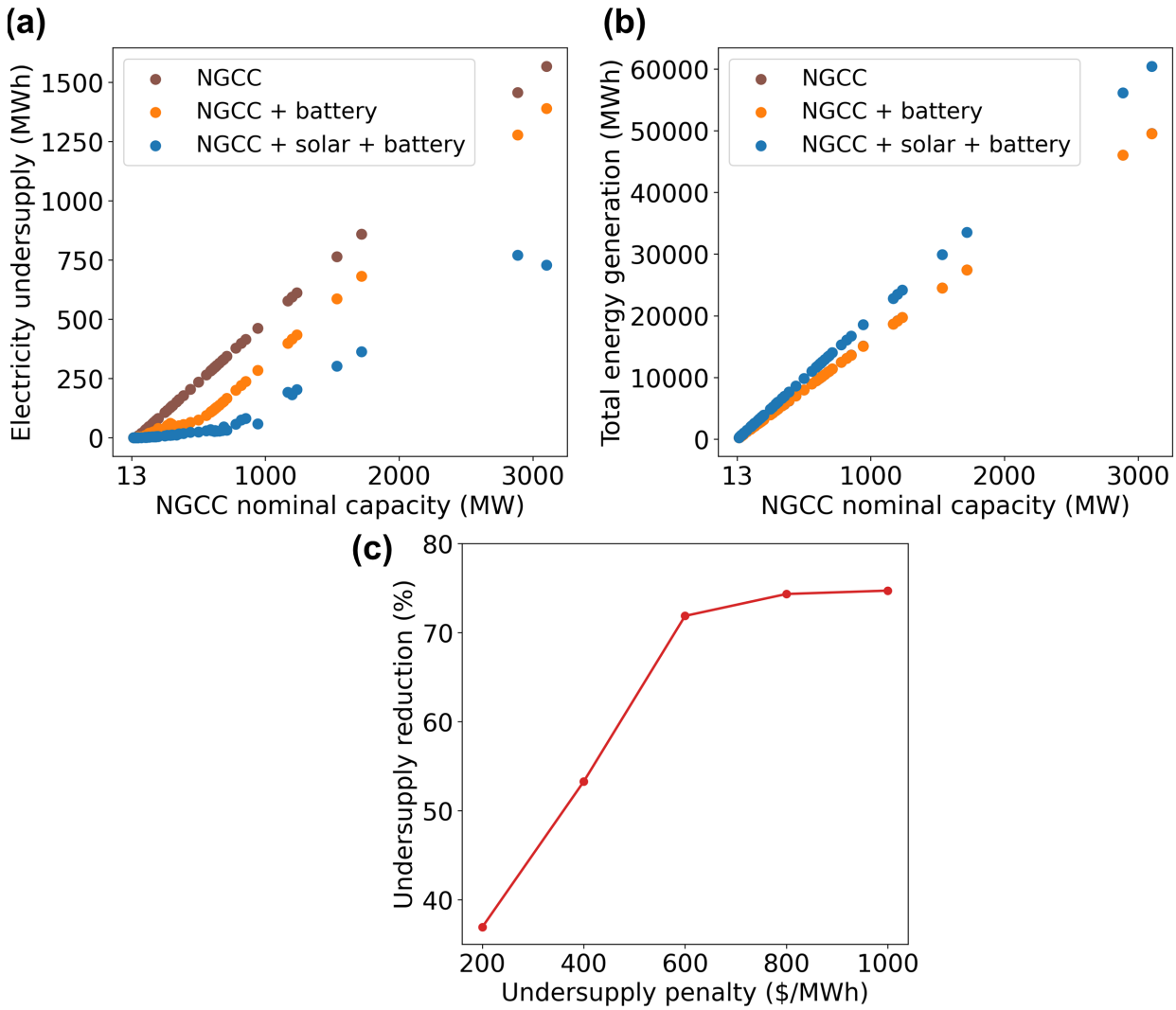

Figure 11: (a) Electricity undersupply comparison, (b) total energy generation comparison for the three configurations, and (c) reduction in average electricity undersupply with increasing penalty. The inclusion of renewable (solar) energy reduces the electricity undersupply of the system while meeting the grid demand, and increases the total energy generation. This results in reduction of the total system cost and the LCOE compared to the case when renewables are not included. The reduction in electricity undersupply obtained from the integration of solar energy and batteries with NGCC plants increases with the penalty imposed on the unmet grid demand.

The comparison of the total energy output and electricity undersupply of the stand-alone NGCC plant, NGCC plant with battery integration, and NGCC plant with battery and localized renewable integration is shown in Figure 11. The total power generated by stand-alone NGCC plants under grid-level renewable integration is the same as that of NGCC plants integrated with batteries.

However, incorporating the localized integration of renewables increases the total energy output and reduces the electricity undersupply. Overall, the localized integration of both batteries and renewables with NGCC plants results in an average of 75% reduction in electricity undersupply compared to the stand-alone NGCC plant for the undersupply penalty of $1000 per MWh. Figure 11c shows the sensitivity analysis of the reduction in the average electricity undersupply with increasing penalty. Overall, we observe that the reduction in the unmet demand obtained from the integration of both renewable energy and battery systems with NGCC power plants increases with the undersupply penalty and varies between 37 - 75%. As the penalty is increased, there is initially a steep increase in the reduction in the undersupply obtained from the integration. This is due to the increase in the battery and renewable farm size. Beyond the undersupply penalty of $600 per MWh, the undersupply plateaus once the maximum limits on the battery and renewable farm sizing are reached. In addition, a 39% reduction in the battery LCOS is achieved from the renewable integration due to reduction in the charging cost.

To evaluate the carbon footprint of the integrated system, we calculate the CO_2 emission intensity. This is defined as the ratio of the total CO_2 emissions of the system to the total energy delivered over the operating horizon. The detailed mathematical representation of the CO_2 emission intensity is shown in Section S4 of the Supplementary Information. We find that the integration of both the battery and the renewable energy reduces the average emission intensity of the NGCC power plants across the state from the base-case emission intensity of 0.44 ton/MWh to 0.36 ton/MWh, or an average reduction of 18%.

Next, we evaluate how the CO_2 emission intensity changes when we also account for the life cycle greenhouse gas emissions of the battery and the solar PV farm. The life cycle emissions represent the 'cradle-to-grave' CO_2 emissions associated with the different stages in the life cycle of the energy system, such as the raw material extraction and the manufacturing, transportation, operation and end-of-life of the battery. As a basis, the unit life cycle emission intensity for the battery is considered to be 33 kg CO_2-eq per MWh of energy discharged. The unit life cycle emission intensity for the solar PV farm is considered to be 46 kg CO_2-eq/MWh.[74–77] We find that the inclusion of the life cycle emissions of the battery and renewable farm in the analysis does not significantly affect the integrated system's CO_2 emission intensity. For instance, the average emission intensity for the integrated 'NGCC + solar + battery' system increases only by about 3% (from 0.36 ton/MWh to 0.37 ton/MWh). Figure 12a demonstrates the resulting emission intensity variation for the various plants across California. The minor increase in the emission intensity of the system on considering the life cycle emissions of the battery and renewable farm is due to the significantly higher emissions associated with the NGCC power plant which outweigh these life cycle emissions. Figure 12b shows the comparison of the emission intensity of the integrated system with the previously considered system of NGCC and battery. The integration of emission-free, clean renewable energy results in an overall 16% reduction in the emission intensity considering the life cycle emissions of the battery and the renewable farm.

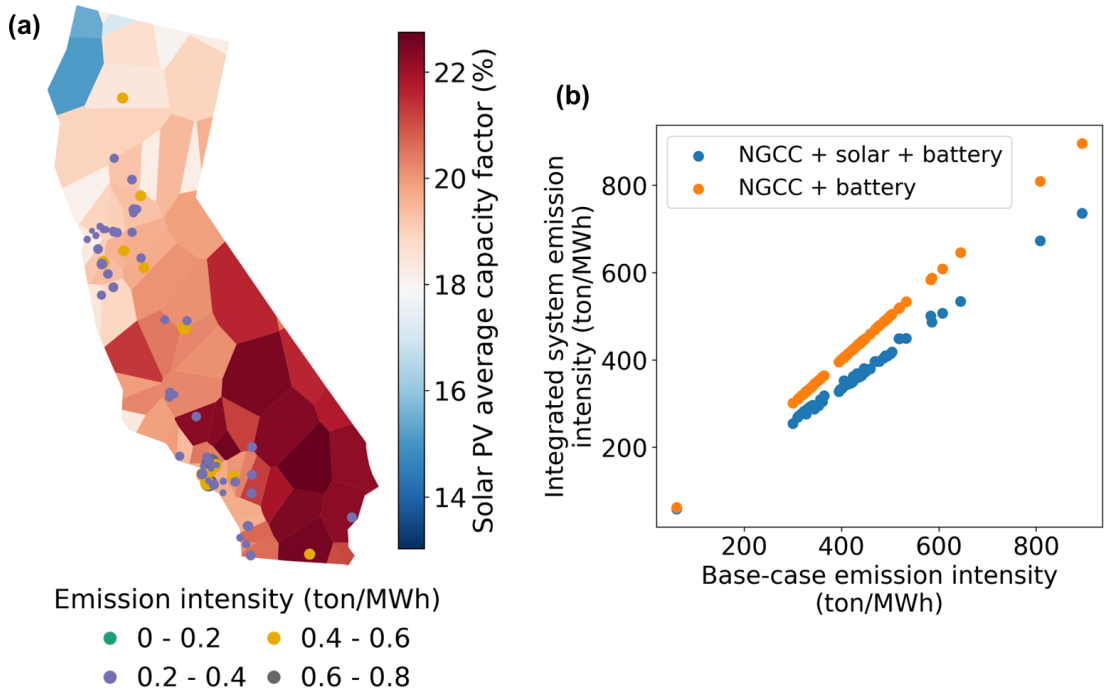

Figure 12: Emission intensity of integrated system of NGCC power plant, renewable energy farm and Li-ion battery shown as (a) spatial variation for the plants across California, and (b) comparison with the integrated system of NGCC plant and battery. Adding renewables to the integrated system results in a reduction in the average emission intensity, with the emission intensity of 48 out of the 65 power plants being in the range of 0.2 - 0.4 ton/MWh compared to the base-case range of 0.4 - 0.6 ton/MWh.

We now ask if it is possible to entirely replace NGCC power plants with renewable energy farms. The upper bound on the renewable farm capacity is taken to be 1.2 times the NGCC plant's nominal capacity, with the same net demand profile. To meet the demand under the variable availability of a renewable farm, a battery is required. The optimal sizes of the renewable energy farms and the battery systems are shown in Figure 13. We find that to mitigate the intermittency of renewables and meet the same demand profile as the NGCC plant, the battery size of 100 MW/400 MWh is not sufficient for 15 out of the 65 plants and larger batteries are required. The battery size increases with the renewable farm size and the solar availability. In addition, the average battery LCOS increases to \$397 per MWh, and the overall system LCOE increases to \$2292 per MWh.

Thus, although the complete replacement of the NGCC power plant with the renewable energy farm results in 100% reduction of CO_2 emissions, the required battery size is significantly high to ensure that the grid demand is met sufficiently. Furthermore, consideration of the electricity over-supply and undersupply costs, as well as the investment cost associated with the renewable energy farm and battery storage results in a high overall system LCOE. Figure 13c shows the renewable energy curtailment for the case of battery integration with the renewable energy plant. We see that the curtailment is nearly twice that of the integration of NGCC plants with renewables and

battery. This indicates that the synergistic integration of batteries and renewables with individual fossil-based units is more beneficial and economical to achieve clean electricity grids as compared to the integration of batteries with stand-alone renewable energy plants which replace the fossil-based units.

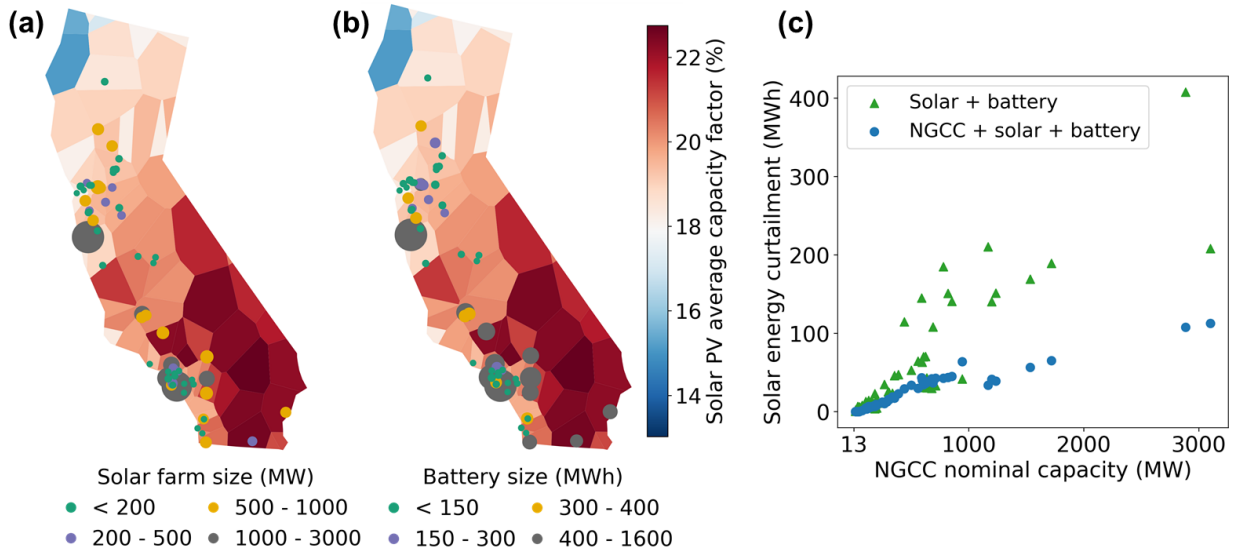

Figure 13: (a) Optimal renewable farm size, (b) optimal battery integration size, and (c) renewable energy curtailment for replacement of NGCC plants with renewable energy farms across the state of California.

4 Conclusions

We departed from the traditional grid-level integration of large-scale energy storage capacities and considered a decentralized integration scheme of energy storage integrated with individual power plants. Specifically, we considered an integrated system of NGCC power plants with storage technologies typically not considered for grid-level integration: electrochemical energy storage in the form of Li-ion and NaS batteries. To determine investment decisions in the battery storage under the spatio-temporal variability of electricity demand and renewable availability, we developed a mathematical programming-based simultaneous design and scheduling framework. The framework determines both the long-term design and the short-term operational decisions for the integrated system to minimize the cost of meeting the time-varying net grid electricity demand. To accurately capture the dynamic interactions between the system components while achieving computational tractability in the resulting large-scale optimization framework, we incorporated equivalent circuit models for the Li-ion battery and time-series reduced-order models for the NaS battery technologies.

The single power plant analysis and the statewide integration studies across California suggest that both the Li-ion and NaS battery integration size increases with the extent of renewable penetration, resulting in a decrease in the LCOS. However, there exists an optimal demand variability increase level beyond which the battery is increasingly overdesigned and the LCOS thereby increases. For the 65 fossil power plants with operating NGCC units in the state of California, the Li-ion technology shows more favorable economics and is the preferred technology for small to medium-sized power plants, while NaS is the optimal technology for larger power plants and at high levels of renewable penetration. Although the investment cost of Li-ion battery is 65% less than that of NaS battery, the lower lifespan of the Li-ion battery technology and the lower storage duration contribute to a statewide average system LCOE with NaS battery integration comparable to the LCOE with Li-ion battery integration.

In addition, we compare the battery integration with NGCC plants alone and the decentralized battery integration with two cases of renewable energy power plants: renewable energy integrated with existing NGCC power plants, and replacement of existing NGCC power plants with renewable energy farms. For the case where the NGCC power plant invests in a battery-enabled co-located renewable energy farm, the total average cost of the system is 18% lower and the LCOE is 31% lower than the integration of battery alone with the NGCC plant. This is due to the additional power output of the renewable farm and the reduction in the electricity undersupply while meeting the peak demand, facilitated by the battery-enabled renewable integration. In addition, the battery LCOS is reduced by 39% as the battery can now be charged using the excess renewable energy which has near-zero marginal production cost. Due to the integration of clean renewable energy, the NGCC plant's emission intensity is reduced by 16%, which includes the life cycle emissions associated with the battery and the renewable energy farm. Furthermore, the proportion of the unmet grid demand is reduced by 75%. The complete replacement of NGCC power plants with

renewable energy farms eliminates the carbon footprint, but requires large battery systems to ensure that the grid demand is met. This significantly increases both the system LCOE and battery LCOS. Furthermore, the average renewable energy curtailment for the battery-enabled renewable integration with NGCC plants is 58% lower than the replacement of NGCC plants with battery-integrated renewable farms. Thus, the localized integration of battery storage and renewable energy with individual fossil power plants is a better alternative to counter the renewable intermittency, as compared to the integration of batteries with stand-alone renewable energy units.

Overall, our analysis shows the advantages of battery-based electrochemical storage to address the issues of renewable intermittency and overgeneration in the state of California. Although Li-ion technology is found to be the best-suited for the decentralized integration, our findings also provide a cost benchmark for NaS batteries to be cost-competitive with the widely popular Li-ion batteries for the utility-scale energy storage application. Future works can consider the effect of the cost evolution of the two battery technologies through learning curves on the integration costs. The economics of the integration with renewable plants will be influenced by the capital cost of the renewable energy power plants, which can be further examined.

As an extension of the analysis presented, carbon capture, utilization and storage (CCUS) can also be considered as an indirect energy storage system to mitigate the renewable intermittency.[30,31] To this end, the following two integration cases can be compared: (i) the integration of renewable energy and CCUS systems with existing fossil power plants, and (ii) the replacement of the existing fossil power plants with battery-integrated renewable energy farms. For the first case, the CCUS system can reduce the CO_2 emissions of the fossil power plants and act as an indirect energy storage system to counter renewable intermittency. Furthermore, the renewable energy system can be used to meet the high energy requirement of CCUS. We have shown that case (ii) eliminates the carbon footprint but requires large-scale energy storage to counter renewable intermittency in the absence of a dispatchable power source. The objective of the systems-level analysis would be to study these trade-offs and determine the best configuration option to reliably meet the grid energy demand in scenarios with an emphasis on carbon reduction.

In addition, this work incorporates conservative operational limits on the battery systems to address the safety concerns associated with the large-scale energy storage. The inclusion of the intricate safety characteristics can be an extension of the current work focusing on a more detailed design and deployment. Future works can also incorporate the battery degradation phenomena through estimation of the battery state of health (SOH). Specifically, for a potential extension of the framework to a capacity-expansion problem, it will be important to also account for battery replacement due to degradation. Although this work considers the integration of batteries primarily with NGCC power plants, the framework can be extended to also study how energy storage adds value to enable the flexible operation of nuclear power plants in electricity grids with significant renewable penetration.

Author Contributions

M.S.Z.: Conceptualization, data curation, formal analysis, investigation, methodology, visualization, software, writing - original draft, writing - review & editing. A.G.: Formal analysis, writing - review & editing. Y.W.: Formal analysis, methodology. S.P.V: Formal analysis, methodology. D.B.: Conceptualization, investigation, supervision, funding acquisition. M.M.F.H.: Conceptualization, investigation, funding acquisition, resources, supervision, writing - review & editing.

Conflicts of Interest

There are no conflicts of interest to declare.

Acknowledgments

The authors gratefully acknowledge funding support from the U.S. Department of Energy (Grant number DE-FE0031771). Part of this research was conducted with the advanced computing resources provided by Texas A&M High Performance Research Computing.

References

[1] U.S. Energy Information Administration, "Today in energy." https://www.eia.gov/todayinenergy/detail.php?id=38752. (accessed May 2021).

[2] California ISO, "What the duck curve tells us about managing a green grid." https://www.caiso.com/documents/flexibleresourceshelprenewables_fastfacts.pdf. (accessed May 2021).

[3] U.S. Department of Energy, "Confronting the duck curve: How to address over-generation of solar energy." https://www.energy.gov/eere/articles/confronting-duck-curve-how-address-over-generation-solar-energy. (accessed May 2021).

[4] P. Denholm and M. Hand, "Grid flexibility and storage required to achieve very high penetration of variable renewable electricity," *Energy Policy*, vol. 39, no. 3, pp. 1817–1830, 2011.

[5] S. Lefton, P. Besuner, and G. Grimsrud, "Managing utility power plant assets to economically optimize power plant cycling costs, life, and reliability," in *Proceedings of International Conference on Control Applications*, pp. 195–208, IEEE, 1995.

[6] K. Van den Bergh and E. Delarue, "Cycling of conventional power plants: technical limits and actual costs," *Energy Conversion and Management*, vol. 97, pp. 70–77, 2015.

[7] A. Benato, S. Bracco, A. Stoppato, and A. Mirandola, "Dynamic simulation of combined cycle power plant cycling in the electricity market," *Energy Conversion and Management*, vol. 107, pp. 76–85, 2016.

[8] Y. Wang, D. Bhattacharyya, and R. Turton, "Evaluation of novel configurations of natural gas combined cycle (NGCC) power plants for load-following operation using dynamic modeling and optimization," *Energy & Fuels*, vol. 34, no. 1, pp. 1053–1070, 2019.

[9] C. F. Heuberger, I. Staffell, N. Shah, and N. Mac Dowell, "A systems approach to quantifying the value of power generation and energy storage technologies in future electricity networks," *Computers & Chemical Engineering*, vol. 107, pp. 247–256, 2017.

[10] D. S. Mallapragada, N. A. Sepulveda, and J. D. Jenkins, "Long-run system value of battery energy storage in future grids with increasing wind and solar generation," *Applied Energy*, vol. 275, p. 115390, 2020.

[11] N. Zhao and F. You, "Can renewable generation, energy storage and energy efficient technologies enable carbon neutral energy transition?," *Applied Energy*, vol. 279, p. 115889, 2020.

[12] M. Trifkovic, W. A. Marvin, P. Daoutidis, and M. Sheikhzadeh, "Dynamic real-time optimization and control of a hybrid energy system," *AIChE Journal*, vol. 60, no. 7, pp. 2546–2556, 2014.

[13] M. J. Palys and P. Daoutidis, "Using hydrogen and ammonia for renewable energy storage: A geographically comprehensive techno-economic study," *Computers & Chemical Engineering*, vol. 136, p. 106785, 2020.

[14] M. Child, C. Kemfert, D. Bogdanov, and C. Breyer, "Flexible electricity generation, grid exchange and storage for the transition to a 100% renewable energy system in europe," *Renewable Energy*, vol. 139, pp. 80–101, 2019.

[15] J. Ramos-Ruiz, B. Wang, H.-M. Chou, P. Enjeti, and L. Xie, "Power electronics intelligence at the network edge (PINE)–an approach to interface PV and battery energy storage systems at the grid edge," *IEEE Journal of Emerging and Selected Topics in Power Electronics*, 2020.

[16] C. D. Demirhan, W. W. Tso, J. B. Powell, and E. N. Pistikopoulos, "A multi-scale energy systems engineering approach towards integrated multi-product network optimization," *Applied Energy*, vol. 281, p. 116020, 2021.

[17] T. M. Gür, "Review of electrical energy storage technologies, materials and systems: challenges and prospects for large-scale grid storage," *Energy & Environmental Science*, vol. 11, no. 10, pp. 2696–2767, 2018.

[18] W. Hausz, B. Berkowitz, and R. Hare, *Conceptual design of thermal energy storage systems for near term electric utility applications*. Department of Energy, Office of Energy Technology, Division of Storage Systems, 1978.

[19] J. D. Wojcik and J. Wang, "Technical feasibility study of thermal energy storage integration into the conventional power plant cycle," *Energies*, vol. 10, no. 2, p. 205, 2017.

[20] M. Mehrpooya, A. Dadak, *et al.*, "Investigation of a combined cycle power plant coupled with a parabolic trough solar field and high temperature energy storage system," *Energy Conversion and Management*, vol. 171, pp. 1662–1674, 2018.

[21] D. Li and J. Wang, "Study of supercritical power plant integration with high temperature thermal energy storage for flexible operation," *Journal of Energy Storage*, vol. 20, pp. 140–152, 2018.

[22] M. Richter, G. Oeljeklaus, and K. Görner, "Improving the load flexibility of coal-fired power plants by the integration of a thermal energy storage," *Applied Energy*, vol. 236, pp. 607–621, 2019.

[23] M. Angerer, S. Kahlert, and H. Spliethoff, "Transient simulation and fatigue evaluation of fast gas turbine startups and shutdowns in a combined cycle plant with an innovative thermal buffer storage," *Energy*, vol. 130, pp. 246–257, 2017.

[24] D. Li, Y. Hu, W. He, and J. Wang, "Dynamic modelling and simulation of a combined-cycle power plant integration with thermal energy storage," in *2017 23rd International Conference on Automation and Computing (ICAC)*, pp. 1–6, IEEE, 2017.

[25] K. Rashid, K. Mohammadi, and K. Powell, "Dynamic simulation and techno-economic analysis of a concentrated solar power (CSP) plant hybridized with both thermal energy storage and natural gas," *Journal of Cleaner Production*, vol. 248, p. 119193, 2020.

[26] R. Kim, Y. Wang, S. P. Vudata, D. Bhattacharyya, F. V. Lima, and R. Turton, "Dynamic optimal dispatch of energy systems with intermittent renewables and damage model," *Mathematics*, vol. 8, no. 6, p. 868, 2020.

[27] M. Vins, J. Dragoun, and M. Sirovy, "Integration of battery energy storage in thermal power plant," in *IECON 2020 The 46th Annual Conference of the IEEE Industrial Electronics Society*, pp. 1608–1613, IEEE, 2020.

[28] M. Zachar, M. Trifkovic, and P. Daoutidis, "Policy effects on microgrid economics, technology selection, and environmental impact," *Computers & Chemical Engineering*, vol. 81, pp. 364–375, 2015.

[29] A. Allman and P. Daoutidis, "Optimal design of synergistic distributed renewable fuel and power systems," *Renewable Energy*, vol. 100, pp. 78–89, 2017.

[30] M. S. Zantye, A. Arora, and M. M. F. Hasan, "Renewable-integrated flexible carbon capture: a synergistic path forward to clean energy future," *Energy & Environmental Science*, vol. 14, pp. 3986–4008, 2021.

[31] M. S. Zantye, M. Li, and M. M. F. Hasan, "Optimal integration of renewables, flexible carbon capture, and energy storage for reducing CO_2 emissions from fossil power plants," in *Computer Aided Chemical Engineering*, vol. 50, pp. 1535–1540, Elsevier, 2021.

[32] M. S. Zantye, A. Arora, and M. M. F. Hasan, "Operational power plant scheduling with flexible carbon capture: A multistage stochastic optimization approach," *Computers & Chemical Engineering*, vol. 130, p. 106544, 2019.

[33] X. Chen, X. Wu, and K. Y. Lee, "The mutual benefits of renewables and carbon capture: Achieved by an artificial intelligent scheduling strategy," *Energy Conversion and Management*, vol. 233, p. 113856, 2021.

[34] H. Sezer, M. Aygun, J. H. Mason, E. Baran, and I. B. Celik, "A computational model for sodium sulfur battery analysis," *ECS Transactions*, vol. 69, no. 1, p. 91, 2015.

[35] M. Doyle, T. F. Fuller, and J. Newman, "Modeling of galvanostatic charge and discharge of the lithium/polymer/insertion cell," *Journal of the Electrochemical Society*, vol. 140, no. 6, p. 1526, 1993.

[36] Z. F. Hussein, W. C. Lee, M. Siam, A. B. Ismail, *et al.*, "Modeling of sodium sulfur battery for power system applications," *Elektrika*, vol. 9, no. 2, pp. 66–72, 2007.

[37] A. Sarasua, M. Molina, D. Pontoriero, and P. Mercado, "Modelling of NAS energy storage system for power system applications," in *2010 IEEE/PES Transmission and Distribution Conference and Exposition: Latin America (T&D-LA)*, pp. 555–560, IEEE, 2010.

[38] L. Sun, G. Li, and F. You, "Combined internal resistance and state-of-charge estimation of lithium-ion battery based on extended state observer," *Renewable and Sustainable Energy Reviews*, vol. 131, p. 109994, 2020.

[39] H. Kawamoto, "Dynamic simulation of the charge-discharge characteristics of the sodium-sulphur cell," *Journal of Applied Electrochemistry*, vol. 21, no. 5, pp. 409–414, 1991.

[40] C. Zhang, Y. Zhu, G. Dong, and J. Wei, "Data-driven lithium-ion battery states estimation using neural networks and particle filtering," *International Journal of Energy Research*, vol. 43, no. 14, pp. 8230–8241, 2019.

[41] H. Chaoui and C. C. Ibe-Ekeocha, "State of charge and state of health estimation for lithium batteries using recurrent neural networks," *IEEE Transactions on Vehicular Technology*, vol. 66, no. 10, pp. 8773–8783, 2017.

[42] F. Yang, X. Song, F. Xu, and K.-L. Tsui, "State-of-charge estimation of lithium-ion batteries via long short-term memory network," *IEEE Access*, vol. 7, pp. 53792–53799, 2019.

[43] C. P. Grey and D. S. Hall, "Prospects for lithium-ion batteries and beyond – a 2030 vision," *Nature Communications*, vol. 11, no. 1, pp. 1–4, 2020.

[44] W. Chen, J. Liang, Z. Yang, and G. Li, "A review of lithium-ion battery for electric vehicle applications and beyond," *Energy Procedia*, vol. 158, pp. 4363–4368, 2019.

[45] T. T. Nguyen, V. Martin, A. Malmquist, and C. A. Silva, "A review on technology maturity of small scale energy storage technologies," *Renewable Energy and Environmental Sustainability*, vol. 2, p. 36, 2017.

[46] N. A. Sepulveda, J. D. Jenkins, F. J. de Sisternes, and R. K. Lester, "The role of firm low-carbon electricity resources in deep decarbonization of power generation," *Joule*, vol. 2, no. 11, pp. 2403–2420, 2018.

[47] Q. Wang, B. Mao, S. I. Stoliarov, and J. Sun, "A review of lithium ion battery failure mechanisms and fire prevention strategies," *Progress in Energy and Combustion Science*, vol. 73, pp. 95–131, 2019.

[48] A. Barré, B. Deguilhem, S. Grolleau, M. Gérard, F. Suard, and D. Riu, "A review on lithium-ion battery ageing mechanisms and estimations for automotive applications," *Journal of Power Sources*, vol. 241, pp. 680–689, 2013.

[49] B. Huang, Z. Pan, X. Su, and L. An, "Recycling of lithium-ion batteries: Recent advances and perspectives," *Journal of Power Sources*, vol. 399, pp. 274–286, 2018.

[50] B. Pattipati, B. Balasingam, G. Avvari, K. Pattipati, and Y. Bar-Shalom, "Open circuit voltage characterization of lithium-ion batteries," *Journal of Power Sources*, vol. 269, pp. 317–333, 2014.

[51] S. Nejad, D. Gladwin, and D. Stone, "A systematic review of lumped-parameter equivalent circuit models for real-time estimation of lithium-ion battery states," *Journal of Power Sources*, vol. 316, pp. 183–196, 2016.

[52] L. Lu, X. Han, J. Li, J. Hua, and M. Ouyang, "A review on the key issues for lithium-ion battery management in electric vehicles," *Journal of Power Sources*, vol. 226, pp. 272–288, 2013.

[53] H. He, R. Xiong, and J. Fan, "Evaluation of lithium-ion battery equivalent circuit models for state of charge estimation by an experimental approach," *Energies*, vol. 4, no. 4, pp. 582–598, 2011.

[54] R. Schröder, M. Aydemir, and G. Seliger, "Comparatively assessing different shapes of lithium-ion battery cells," *Procedia Manufacturing*, vol. 8, pp. 104–111, 2017.

[55] H. Kawamoto and Y. Kusakabe, "Performance and thermal behavior of sodium-sulfur cell

under high current density operations," *Journal of the Electrochemical Society*, vol. 136, no. 5, p. 1355, 1989.

[56] M. McKubre, F. Tanzella, and S. Smedley, "The electromotive force of the Na/S cell," *Journal of the Electrochemical Society*, vol. 136, no. 2, p. 303, 1989.

[57] Z. Wen, J. Cao, Z. Gu, X. Xu, F. Zhang, and Z. Lin, "Research on sodium sulfur battery for energy storage," *Solid State Ionics*, vol. 179, no. 27-32, pp. 1697–1701, 2008.

[58] T. M. Letcher, R. Law, and D. Reay, *Storing energy: with special reference to renewable energy sources*, vol. 86. Elsevier Amsterdam, 2016.

[59] D. W. Gao, *Energy storage for sustainable microgrid*. Academic Press, 2015.

[60] K. B. Hueso, M. Armand, and T. Rojo, "High temperature sodium batteries: status, challenges and future trends," *Energy & Environmental Science*, vol. 6, no. 3, pp. 734–749, 2013.

[61] T. Oshima, M. Kajita, and A. Okuno, "Development of sodium-sulfur batteries," *International Journal of Applied Ceramic Technology*, vol. 1, no. 3, pp. 269–276, 2004.

[62] J. Sudworth and A. Tiley, *Sodium sulphur battery*. Springer Science & Business Media, 1985.

[63] S. P. Vudata and D. Bhattacharyya, "Thermal management of a high temperature sodium sulphur battery stack," *International Journal of Heat and Mass Transfer*, vol. 181, p. 122025, 2021.

[64] S. Schaefer, S. P. Vudata, D. Bhattacharyya, and R. Turton, "Transient modeling and simulation of a nonisothermal sodium–sulfur cell," *Journal of Power Sources*, vol. 453, p. 227849, 2020.

[65] D. Bhattacharyya and R. Rengaswamy, "System identification and nonlinear model predictive control of a solid oxide fuel cell," *Industrial & Engineering Chemistry Research*, vol. 49, no. 10, pp. 4800–4808, 2010.

[66] D. S. Mallapragada, E. Gençer, P. Insinger, D. W. Keith, and F. M. OSullivan, "Can industrial-scale solar hydrogen supplied from commodity technologies be cost competitive by 2030?," *Cell Reports Physical Science*, vol. 1, no. 9, p. 100174, 2020.

[67] U.S. Energy Information Administration, "State profile and energy estimates: California." `https://www.eia.gov/state/analysis.php?sid=CA#75`. (accessed June 2021).

[68] California ISO, "Today's outlook." `http://www.caiso.com/TodaysOutlook/Pages/default.aspx`. (accessed May 2021).

[69] U.S. Environmental Protection Agency (EPA), "Emissions & generation resource integrated database (eGRID)." `https://www.epa.gov/egrid`. (accessed August 2021).

[70] U.S. Energy Information Administration, "How much carbon dioxide is produced per kilowatthour of U.S. electricity generation?." `https://www.eia.gov/tools/faqs/faq.php?id=74&t=11`. (accessed March 2021).

[71] National Renewable Energy Laboratory (NREL), "National Solar Radiation Database." `https://nsrdb.nrel.gov/`. (accessed May 2020).

[72] A. Arora, M. S. Zantye, and M. M. F. Hasan, "Sustainable hydrogen manufacturing via renewable-integrated intensified process for refueling stations," *Applied Energy*, vol. 311, p. 118667, 2022.

[73] W. M. Seong, K.-Y. Park, M. H. Lee, S. Moon, K. Oh, H. Park, S. Lee, and K. Kang, "Abnormal self-discharge in lithium-ion batteries," *Energy & Environmental Science*, vol. 11, no. 4, pp. 970–978, 2018.

[74] National Renewable Energy Laboratory (NREL), "Life cycle greenhouse gas emissions from electricity generation: Update." `https://www.nrel.gov/docs/fy21osti/80580.pdf`. (accessed June 2022).

[75] H. C. Kim, V. Fthenakis, J.-K. Choi, and D. E. Turney, "Life cycle greenhouse gas emissions of thin-film photovoltaic electricity generation: Systematic review and harmonization," *Journal of Industrial Ecology*, vol. 16, pp. S110–S121, 2012.

[76] R. Yudhistira, D. Khatiwada, and F. Sanchez, "A comparative life cycle assessment of lithium-ion and lead-acid batteries for grid energy storage," *Journal of Cleaner Production*, vol. 358, p. 131999, 2022.

[77] Y. Liang, J. Su, B. Xi, Y. Yu, D. Ji, Y. Sun, C. Cui, and J. Zhu, "Life cycle assessment of lithium-ion batteries for greenhouse gas emissions," *Resources, Conservation and Recycling*, vol. 117, pp. 285–293, 2017.